RSC Advances

PAPER

View Article Online
View Journal | View Issue

Cite this: *RSC Adv.*, 2023, **13**, 33114

Enhancing the electrocatalytic performance of SnX_2 (X = S and Se) monolayers for CO_2 reduction to HCOOH *via* transition metal atom adsorption: a theoretical investigation†

Feifei Xia, Qing Xu, Fengli Yang, Li Shu and Yingpin Wen

Exploring highly efficient, stable, and low-cost electrocatalysts for CO_2 reduction reaction (CRR) can not only mitigate greenhouse gas emission but also store renewable energy. Herein, CO_2 electroreduction to HCOOH on the surface of SnX_2 (X = S and Se) monolayer-supported non-noble metal atoms (Fe, Co and Ni) was systematically investigated using first-principles calculations. Our results show that Fe, Co and Ni adsorbed on the surface of SnX_2 (X = S and Se) monolayers can effectively enhance their electrocatalytic activity for CO_2 reduction to HCOOH with low limiting potentials due to the decreasing energy barrier of *OOCH. Moreover, the lower free energy of the *OOCH intermediate on the surface of TM/SnX_2 (X = S and Se) monolayers verifies that the electroreduction of CO_2 to HCOOH prefers to proceed along the path: CO_2 → *OOCH → *HCOOH → HCOOH. Interestingly, SnX_2 (X = S and Se) monolayer-supported Co and Ni atoms prefer the HCOOH product with low CRR overpotentials of 0.03/0.01 V and 0.13/0.05 V, respectively, showing remarkable catalytic performance. This work reveals an efficient strategy to enhance the electrocatalytic performance of SnX_2 (X = S and Se) monolayers for CO_2 reduction to HCOOH, which could provide a way to design and develop new CRR catalysts experimentally in future.

Received 2nd October 2023
Accepted 6th November 2023

DOI: 10.1039/d3ra06692d

rsc.li/rsc-advances

1. Introduction

Nowadays, the greenhouse effect and energy shortage have become more serious with the rapid worldwide economic expansion, and threaten the survival and development of mankind.[1,2] So mitigating CO_2 emissions and converting CO_2 into valuable products have attracted great research attention due to the potential impact on energy storage and recycling resources.[3] The electrocatalytic CO_2 reduction reaction (CRR) has been widely studied experimentally and theoretically,[4–10] which not only reduces CO_2 emissions but also simultaneously produces valuable chemicals, such as the main C1 products HCOOH, CO, CH_3OH and CH_4. However, it is challenging to explore efficient electrocatalysts to improve the exothermic CRR process due to the inert nature of CO_2.[11,12] In addition, there are some severe bottleneck issues in the process of CRR, such as various intermediates and many reduction reaction pathways, leading to poor product selectivity as well as loss of efficiency toward the competing hydrogen evolution.[13–15] Therefore, it is very necessary to design and synthesize electrocatalysts with high product selectivity, low limiting potential and eminent catalytic performance for CRR.

It has been reported that Sn-based catalysts have been found with superior performance toward CRR because of their high activity and selectivity.[8,9,16–25] Generally, the *OOCH intermediate is more favorable for Sn-based catalysts during CRR because CO_2 prefers to form a bidentate O–Sn adsorption configuration on Sn sites, which results in the HCOOH product, corresponding to a two-electron transfer mechanism. For example, Guan *et al.*[8,9] fabricated metal tin and tin oxides catalysts by different electrodeposition methods and revealed that these catalysts had efficient catalytic ability for CO_2 electroreduction to HCOOH. Geng *et al.*[22] demonstrated the catalytic activity of SnS_2 nanosheets for CRR was obviously enhanced by surface hydrogen incorporation, which decreases the energy barrier of *OOCH intermediate formation and is in favor of HCOOH product. He *et al.*[24] synthesized a $SnSe_2$@CC electrocatalyst that is high selectivity and catalytic activity towards HCOOH production. All these reported works show that the catalytic performance of two-dimensional (2D) SnX_2 (X = S and Se) for CRR can be modulated by surface modification.

In the other hand, single-atom catalysts (SACs) are prospective CRR electrocatalysts because SACs characterized by an isolated metal atom supported on the solid surface play important roles in activating substrate materials.[26–32] For

School of Chemistry and Chemical Engineering, Jiangsu University of Technology, Changzhou 213001, Jiangsu, P. R. China. E-mail: ffxia@jsut.edu.cn

† Electronic supplementary information (ESI) available. See DOI: https://doi.org/10.1039/d3ra06692d

example, Xie *et al.*[28] reported that Co atoms on the surface of atomically thin layers prefer to form *OOCH intermediate during CRR with higher activity and selectivity towards HCOOH product. Zheng and co-workers[29] synthesized a low-cost carbon nanoparticle supported Ni single atoms *via* a simple and scalable method, which is high selective and active toward CO production. Moreover, 2D materials supported transition metal (TM) atoms have been supposed as efficient electrocatalyst for CRR due to their large surface-to-volume ratio, tunable electronic structures and strong coordinating capability.[30–32] Thus, inspired by these reported works, whether TM atoms anchored on the surface of SnX_2 (X = S and Se) monolayers could also improve the catalytic performance of these monolayers for CRR or not, which is necessary to gain an insight into the relationship between the TM atoms and SnX_2 (X = S and Se) monolayers and screens out the optimal electrocatalysts for HCOOH production.

Herein, the SnX_2 (X = S and Se) monolayers before and after supported Fe, Co and Ni atoms for CO_2 electroreduction to HCOOH were systematically investigated by first-principles calculation based on density functional theory (DFT)[33,34] in the work. Considering the competition of hydrogen evolution reaction (HER) and CRR, the Gibbs free energies of *H, *COOH and *OOCH intermediates were calculated, which is plotted by $\Delta G_{*\mathrm{COOH}/*\mathrm{OOCH}}$ *versus* $\Delta G_{*\mathrm{H}}$. The results show that SnX_2 (X = S and Se) monolayers supported Fe, Co and Ni atoms tend to form *OOCH intermediate, leading to the HCOOH production. Moreover, the overpotential and limiting potential calculations revealed that the electrocatalytic performance of SnX_2 (X = S and Se) monolayers for CO_2 reduction to HCOOH can be obviously improved by adsorption of Fe, Co and Ni atoms. Especially, Co and Ni anchored on SnX_2 (X = S and Se) monolayers for HCOOH production with the lower overpotentials and limiting potentials, corresponding to the potential determining step of $*+ CO_2 \rightarrow *CO_2$. Our calculated results are beneficial to synthesize more efficient CRR catalysts in future, which would provide a perspective on the phenomena observed in the experiment.

2. Computational methods

All the geometry optimization and energy calculations were performed using the Vienna *ab initio* simulation package (VASP)[35,36] based on the DFT with the Perdew–Burke–Ernzerhof (PBE) functional for generalized gradient approximation (GGA)[37–39] to characterize the electron exchange and correlation effects. The van der Waals interaction was described in Grimme's scheme (DFT-D3).[40] A cutoff energy of 500 eV was used for the plane-wave basis set, and the energy and force convergence criteria were set to 10^{-6} eV and 0.01 eV $Å^{-1}$, respectively. The vacuum space of 18 Å was chosen to avoid the interaction between the periodical images. Brillouin zone sampling is performed with Monkhorst–Pack special *k*-point meshes,[41] and the $6 \times 6 \times 1$ *k*-grid was chosen for the geometry optimization of SnX_2 (X = S and Se) monolayers.

The adsorption energy (E_{ads}) of reaction intermediate (*A*) on the surface of different SnX_2 (X = S and Se) monolayers was defined as:

$$E_{\mathrm{ads}} = E_{*\mathrm{adsorbate}} - E_{*} - E_{\mathrm{adsorbate}} \quad (1)$$

where $E_{*\mathrm{adsorbate}}$, E_{*} and $E_{\mathrm{adsorbate}}$ are the total energy of the adsorbate on the surface of catalyst, the catalyst and the adsorbate, respectively.

Free energies of the CRR intermediates in electrochemical reaction pathways were evaluated according to the computational hydrogen electrode (CHE) model developed by Nørskov *et al.*[42,43] using the reversible hydrogen electrode (RHE) as a reference which chemical potential of $(H^+ + e^-)$ is equivalent to that of $1/2H_2$ at 0 V and at all pH values. In the acidic condition, the mechanism of CO_2 reduction to HCOOH is generally regarded as the following steps:[8,9]

$$*+ CO_2 + H^+ + e^- \rightarrow *\mathrm{COOH} \quad (2)$$

$$*\mathrm{COOH} + H^+ + e^- \rightarrow *+ \mathrm{HCOOH} \quad (3)$$

$$*+ CO_2 + H^+ + e^- \rightarrow *\mathrm{OOCH} \quad (4)$$

$$*\mathrm{OOCH} + H^+ + e^- \rightarrow *+ \mathrm{HCOOH} \quad (5)$$

Thus, the Gibbs free energies of each intermediate were calculated as:[42]

$$\Delta G = \Delta E - \Delta E_{\mathrm{ZPE}} - T\Delta S + \Delta G_U + \Delta G_{\mathrm{pH}} \quad (6)$$

where ΔE, ΔE_{ZPE} and $T\Delta S$ are the total calculated energies, zero-point energy corrections and entropy contributions at 298.15 K, respectively. ΔG_U is the free energy change of electrode potential (U). ΔG_{pH} is the free energy correction relating to the solution pH (in this paper pH = 0 for acidic medium). The less negative limiting potential (U_{L}), the higher activity and selectivity of the catalysts, so U_{L} determined by the potential determining steps (PDS) is obtained from the free energy change (ΔG_{MAX}) by using the relation $U_{\mathrm{L}} = -\Delta G_{\mathrm{MAX}}/ne$. Moreover, the overpotential (η) is calculated to evaluate the catalytic performance of different SnX_2 (X = S and Se) monolayers, which is the difference between the equilibrium potential (U_{e}) and U_{L}. The vibrational frequency of intermediates for CRR by VASPKIT software that is a pre and post-processing program.[44]

3. Results and discussion

3.1 Adsorption of *H, *COOH and *OOCH

It is well known that the hydrogen evolution reaction (HER) is a competitive reaction during the process of CRR on the most of metal catalysts due to the selectivity of first protonation step.[45,46] Therefore, we firstly calculated the *H, *COOH and *OOCH intermediates adsorption on the surface of SnX_2 (X = S and Se) monolayers, and the corresponding optimized energy favorable structures are presented in Fig. 1 and S1.† In accordance with our previous work,[47] the transition metal

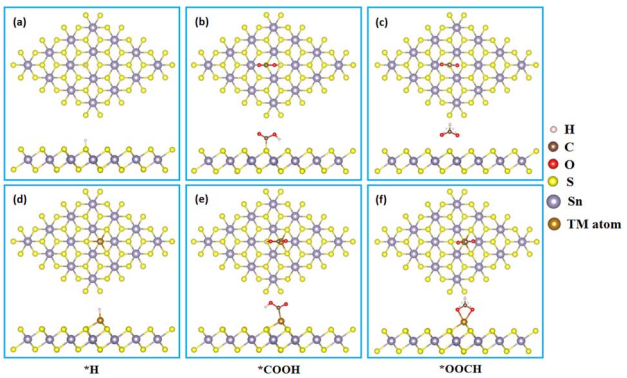

Fig. 1 Side and top views of key intermediates (*H, *COOH and *OOCH) adsorption on the surface of (a–c) pristine SnS_2 and (d–f) TM/SnS_2 monolayers.

atoms (Fe, Co and Ni) also prefer to anchor on the six-member ring (hollow) site of $SnSe_2$ monolayers (Fig. S1†).

It can be noted that the E_{ads} of *H, *COOH and *OOCH intermediates absorbed on pristine SnX_2 (X = S and Se) monolayers are above zero as shown in Fig. 2, indicating unfavorable adsorption. In contrary, the adsorption of *COOH and *OOCH intermediates on the surface of TM/SnX_2 (X = S and Se) monolayers are strengthened, especially the *OOCH adsorption, which reveals that the first protonation step tends to form *COOH and *OOCH intermediates for the CRR. In addition, the adsorption of CO_2, H_2O, CO, and HCOOH molecules on the surface of SnX_2 (X = S and Se) monolayers was calculated to evaluate the interaction between these small molecules and the monolayers. As shown in Fig. S2 and Table S1,† the distinct difference in adsorption energies among CO_2, H_2O, CO, and HCOOH due to the presence of active site on SnX_2 (X = S and Se) monolayers, indicating the selectivity of CRR.

3.2 Selectivity between CRR and HER

As mentioned above, there is a competition to form *COOH, *OOCH and *H intermediates in the first protonation step for CRR. In addition, it is reported that the reaction with lower free energy is assumed to be more selective with a low reaction barrier.[48–51] Therefore, the Gibbs free energies of *COOH, *OOCH and *H absorbed on SnX_2 (X = S and Se) monolayers were calculated and compared (shown in Fig. 3)

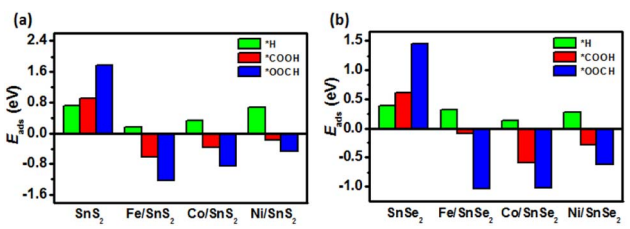

Fig. 2 The adsorption energy (E_{ads}) of key intermediates (*H, *COOH and *OOCH) adsorption on the surface of (a) SnS_2 and (b) $SnSe_2$ monolayers.

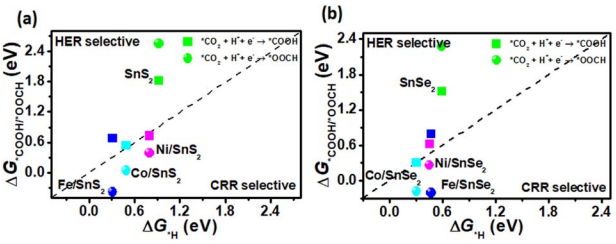

Fig. 3 The free energy change of the first protonation step in the CRR and HER on the surface of (a) SnS_2 and (b) $SnSe_2$ monolayers.

to gain an insight into the selectivity of the catalysts for CRR and HER, respectively. As shown in Fig. 3, the Gibbs free energy change of *COOH and *OOCH (ΔG_{*COOH} and ΔG_{*OOCH}) *versus* that of *H (ΔG_{*H}) was plotted, and usually the electrocatalysts under the dotted line are CRR selective, while above the dotted line are HER selective. For all TM/SnX_2 (X = S and Se) monolayers, *OOCH is more favorable than *COOH and they are below the diagonal line, implying that TM/SnX_2 (X = S and Se) monolayers prefer to form *OOCH in the first protonation step for CRR rather than *COOH and *H, and leading to the inhibition of HER. However, pristine SnX_2 (X = S and Se) monolayers are above the diagonal line, meaning more selective for HER. And the free energy barriers of the formation of *COOH and *OOCH for pristine SnX_2 (X = S and Se) monolayers are higher than 1 eV, revealing that the CRR is difficult. In contrary, the free energy barriers of *OOCH and *COOH are obvious decreased for TM/SnX_2 (X = S and Se) monolayers, especially the free energy of *OOCH is 0.04 eV, which exhibits that TM atoms (Fe, Co and Ni) anchored on the surface of SnX_2 (X = S and Se) monolayers is an effective strategy to improve the catalytic activity for CRR.

3.3 Electrocatalytic activity

In order to gain a clearer understanding of the electrocatalytic performance and mechanism of TM/SnX_2 (X = S and Se) monolayers for CO_2 reduction to HCOOH, the Gibbs free energies of all possible intermediates for CRR were systematically calculated and the corresponding configurations presented in Fig. S3 and S4.† The possible reaction pathways of CRR with two

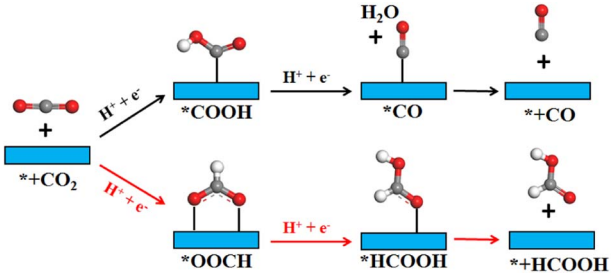

Fig. 4 Schematic illustration of CO_2 reduction to HCOOH and CO products on the surface of SnX_2 (X = S and Se) monolayers. The gray, red and white atoms represent C, O and H, respectively.

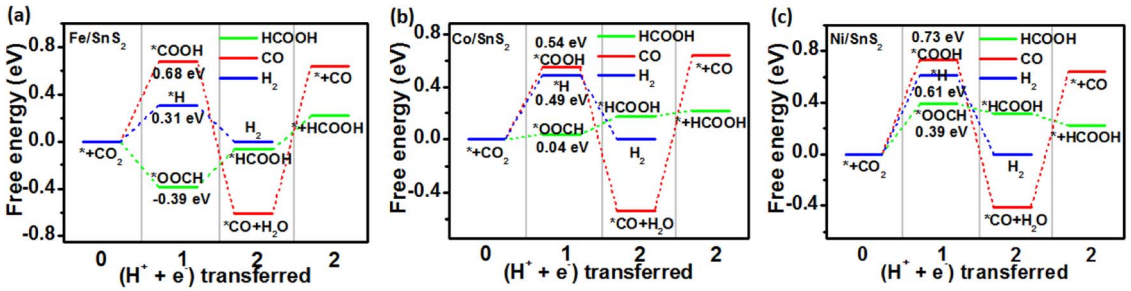

Fig. 5 Free energy diagram for electroreduction of CO_2 to HCOOH (green), CO (red) and H_2 (blue) on the surface of (a) Fe/SnS_2, (b) Co/SnS_2 and (c) Ni/SnS_2 monolayers.

electrons transfers are illustrated in Fig. 4, which have been widely accepted for the tin-based electrocatalysts.[8,9,21–25] And the lower free energy of *OOCH intermediate on the surface of TM/SnX_2 (X = S and Se) monolayers also verifies the electroreduction of CO_2 to HCOOH prefers to proceed along CO_2 → *OOCH → *HCOOH → HCOOH (Fig. 5 and 6). However, there are high free energy barrier of *COOH for CO_2 reduction to HCOOH and CO over the pristine SnX_2 (X = S and Se) monolayers (as shown in Fig. S5†), indicating the unfavorable electrocatalytic performance for CRR.

As shown in Fig. 5 and 6, the calculated energy barrier of *OOCH is lower than those of *H and *COOH, revealing the selectivity of TM/SnX_2 (X = S and Se) monolayers for CO_2 electroreduction to HCOOH. It can be noted that Fe, Co and Ni atoms anchored on the surface of SnX_2 (X = S and Se) monolayers for CRR favor to form *OOCH intermediate with a much smaller free energies compared to form *COOH and *H intermediates in the first protonation step. For the second protonation step, the reaction proceeds from *OOCH to *HCOOH for Ni/SnX_2 (X = S and Se) monolayers is exothermic, indicating a spontaneous process. In contrast, this protonation process for other monolayers is endothermic, which reveal that this step cannot spontaneously occur. Interestingly, the activation energy was found to be 0.04 eV for CO_2 → *OOCH on Co/SnS_2, and the subsequent step of *OOCH → *HCOOH and *HCOOH → HCOOH also owns small barrier of about 0.21 and 0.02 eV, respectively. However, the energy barrier of CO_2 to *OOCH and *COOH on the pristine SnX_2 (X = S and Se) monolayers is above 1.5 eV (Fig. S5†), which is not beneficial for the formation of HCOOH. Moreover, the free energy of *H for HER on TM/SnX_2 (X = S and Se) is much higher than that of *OOCH for CRR, confirms the selectivity of CRR over HER. The Fig. S6 and S7† also exhibit that Fe, Co and Ni atoms anchored on the surface of SnX_2 (X = S and Se) monolayers can obviously narrow the free energy barrier of the first protonation step ($* + CO_2 + H^+ + e^- \rightarrow$ *OOCH) in CRR, which is beneficial to improve the electrocatalytic activity for CO_2 reduction to HCOOH. Meanwhile, Our calculated results also show that the free energy barrier (from $*CO + H^+ + e^-$ to *CHO) is high in this protonation step during CRR for TM/SnX_2 (X = S and Se) monolayers (shown in Fig. S8†), indicating unfavorable formation of formaldehyde and methanol product.

3.4 Limiting potential and product selectivity

It has been reported that the limiting potential difference (*i.e.*, $U_L(CO_2) - U_L(H_2)$, where $U_L = -\Delta G_{max}/e$) can be used as a reasonable selectivity descriptor for CRR and HER.[52–54] Usually, the more positive $U_L(CO_2) - U_L(H_2)$ value corresponds to the more favorable CRR selectivity. Therefore, to further evaluate the CRR and HER selectivity on different SnX_2 (X = S and Se) monolayers, the limiting potential difference (ΔU_L) at zero applied potential and acidic condition was calculated and compared. As clearly seen in Fig. 7, the ΔU_L for CO_2 to HCOOH is positive on the surface of SnX_2 (X = S and Se) monolayers supported Co and Ni atoms, signifying a higher HCOOH selectivity for CRR. In contrast, the pristine SnX_2 (X = S and Se) monolayers exhibit worse CRR selectivity without applied potential (U = 0.0 V *versus* RHE). As the Fe atom anchored on

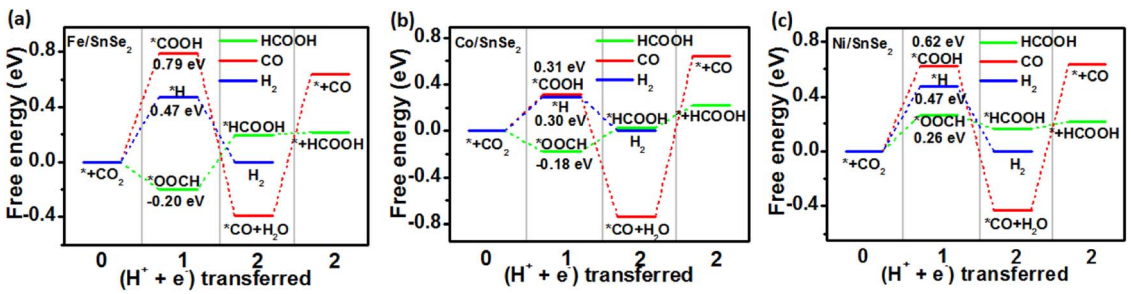

Fig. 6 Free energy diagram for electroreduction of CO_2 to HCOOH (green), CO (red) and H_2 (blue) on the surface of (a) $Fe/SnSe_2$, (b) $Co/SnSe_2$ and (c) $Ni/SnSe_2$ monolayers.

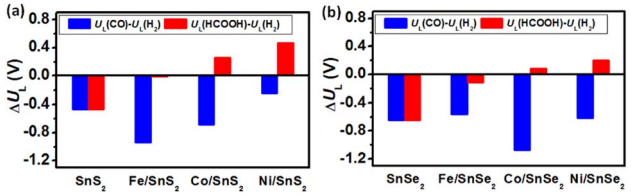

Fig. 7 Limiting potential differences (U_L(CO) − U_L(H$_2$) and U_L(-HCOOH) − U_L(H$_2$)) between CRR and HER on the surface of different (a) SnS_2 and (b) $SnSe_2$ monolayers at 0 V *vs.* RHE.

Table 1 The potential determining steps (PDS), limiting potentials ($U_L = -\Delta G_{max}/e$) and overpotentials ($\eta = U_{equ} - U_L$, U_{equ} is the equilibrium potential) for CO_2 reduction to HCOOH on the different surface of SnX_2 (X = S and Se) monolayers

Surface	PDS	U_L/V	η/V
Pristine SnS_2	*CO_2 → *COOH	−1.39	1.19
Fe/SnS_2	*COOH → *HCOOH	−0.32	0.12
Co/SnS_2	*+ CO_2 → *CO_2	−0.23	0.03
Ni/SnS_2	*+ CO_2 → *CO_2	−0.33	0.13
Pristine $SnSe_2$	*CO_2 → *COOH	−1.24	1.04
Fe/$SnSe_2$	*+ CO_2 → *CO_2	−0.59	0.39
Co/$SnSe_2$	*OOCH → *HCOOH	−0.21	0.01
Ni/$SnSe_2$	*+ CO_2 → *CO_2	−0.25	0.05

SnX_2 (X = S and Se), the ΔU_L for HCOOH route becomes nearly zero, suggesting the obvious effect of suppressing HER. In addition, the calculated limiting potential difference of U_L(-CO)−U_L(H$_2$) is negative for all SnX_2 (X = S and Se) monolayers, which indicates worse CRR selectivity for CO production.

The potential determining steps (PDS), limiting potentials (U_L) and overpotentials (η) for CO_2 reduction to HCOOH and CO were summarized in Tables 1 and S2,† respectively. It can be noted that the free energy changes of PDS for pristine SnS_2 and $SnSe_2$ are obvious higher than those of TM/SnX_2 (X = S and Se), and the high overpotentials for CO_2 reduction to HCOOH and CO reveal poor CRR selectivity. In contrast, the electrocatalytic activity of SnX_2 (X = S and Se) monolayers supported Fe, Co and Ni atoms for CO_2 to HCOOH production is distinctly enhanced with lower overpotentials, but for CO formation displaying inferior catalytic activity. Especially, the Ni/SnX_2(X = S and Se) monolayers are supposed to be superior in catalyzing CO_2 to HCOOH based on U_L and η calculated from free energy changes of PDS, where *+ CO_2 → *CO_2 is predicted to be the PDS. All these results illustrate that the adsorption of Fe, Co and Ni atoms on the surface of SnX_2 (X = S and Se) monolayers can effectively tune the catalytic activity for CRR, which would provide an insight to the selective electroreduction of CO_2 based on the materials in the future experiment.

4. Conclusions

In summary, the electrocatalytic activity of pristine and TM atoms (Fe, Co and Ni) anchored on SnX_2 (X = S and Se) monolayers for CO_2 reduction to HCOOH were systematically investigated by first-principles calculation method. The calculated free energies of *COOH, *OOCH and *H reveal that it is easier to form *OOCH intermediate in the first protonation step of CRR on the SnX_2 (X = S and Se) monolayers supported Fe, Co and Ni atoms. Meanwhile, the electrocatalytic activity of SnX_2 (X = S and Se) monolayers for CO_2 reduction to HCOOH can be obviously promoted by TM atoms (Fe, Co and Ni) adsorption, which confirms the selectivity of CRR over HER. Moreover, the calculated limiting potential differences (ΔU_L) display that the adsorption of Co and Ni on SnX_2 (X = S and Se) monolayers prefers a higher HCOOH selectivity for CRR with lower overpotentials, while pristine SnX_2 (X = S and Se) monolayers exhibit worse CRR selectivity with higher overpotentials both for HCOOH and CO production. All these results demonstrate that TM atoms (Fe, Co and Ni) own great potential of enhancing the electrocatalytic performance of SnX_2 (X = S and Se) monolayers for CO_2 reduction to HCOOH, which can provide a theoretical reference for designing high-efficiency SnX_2 (X = S and Se)-based single atom catalysts experimentally in future.

Conflicts of interest

There are no conflicts to declare.

Acknowledgements

This work was supported by the National Natural Science Foundation of China (No. 21703087).

Notes and references

1 D. R. Yang, B. Ni and X. Wang, *Adv. Energy Mater.*, 2020, **10**, 2001142.
2 R. Ahmed, G. J. Liu, B. Yousaf, Q. Abbas, H. Ullah and M. U. Ali, *J. Cleaner Prod.*, 2020, **242**, 118409.
3 A. Vasileff, Y. Zheng and S. Z. Qiao, *Adv. Energy Mater.*, 2017, **7**, 1700759.
4 R. Kortlever, J. Shen, K. J. P. Schouten, F. Calle-Vallejo and M. T. M. Koper, *J. Phys. Chem. Lett.*, 2015, **6**, 4073–4082.
5 D. D. Zhu, J. L. Liu and S. Z. Qiao, *Adv. Mater.*, 2016, **28**, 3423–3452.
6 C. W. Li, J. Ciston and M. W. Kanan, *Nature*, 2014, **508**, 504–507.
7 Z. Y. Sun, T. Ma, H. C. Tao, Q. Fan and B. X. Han, *Chem*, 2017, **3**, 560–587.
8 X. W. An, S. S. Li, A. Yoshida, T. Yu, Z. D. Wang, X. G. Hao, A. Abudula and G. Q. Guan, *ACS Appl. Mater. Interfaces*, 2019, **11**, 42114–42122.
9 X. W. An, S. S. Li, A. Yoshida, Z. D. Wang, X. G. Hao, A. Abudula and G. Q. Guan, *ACS Sustainable Chem. Eng.*, 2019, **7**, 9360–9368.
10 L. L. Gong, D. T. Zhang, C. Y. Lin, Y. H. Zhu, Y. Shen, J. Zhang, X. Han, L. P. Zhang and Z. H. Xia, *Adv. Energy Mater.*, 2019, **44**, 1902625.

11 K. Jiang, R. B. Sandberg, A. J. Akey, X. Liu, D. C. Bell, J. K. Nørskov, K. Chan and H. Wang, *Nat. Catal.*, 2018, **1**, 111–119.
12 E. E. Benson, C. P. Kubiak, A. J. Sathrum and J. M. Smieja, *Chem. Soc. Rev.*, 2009, **38**, 89–99.
13 R. Francke, B. Schille and M. Roemelt, *Chem. Rev.*, 2018, **118**, 4631–4701.
14 O. Melchaeva, P. Voyame, V. C. Bassetto, M. Prokein, M. Renner, E. Weidner, M. Petermann and A. Battistel, *ChemSusChem*, 2017, **10**, 3660–3670.
15 R. J. Lim, M. S. Xie, M. A. Sk, J.-M. Lee, A. Fisher, X. Wang and K. H. Lim, *Catal. Today*, 2014, **233**, 169–180.
16 C. Zhao and J. Wang, *Chem. Eng. J.*, 2016, **293**, 161–170.
17 L. Fan, Z. Xia, M. J. Xu, Y. Y. Lu and Z. J. Li, *Adv. Funct. Mater.*, 2018, **28**, 1706289.
18 J. Gu, F. Héroguel, J. Luterbacher and X. Hu, *Angew. Chem.*, 2018, **130**, 2993–2997.
19 F. Li, L. Chen, M. Xue, T. Williams, Y. Zhang, D. R. MacFarlane and J. Zhang, *Nano Energy*, 2017, **31**, 270–277.
20 Y. Luo, Y. Cui, M. Y. Li, X. L. Zhang, Y. X. Dai, C. Y. Ling and Y. C. Huang, *ACS Appl. Nano Mater.*, 2021, **4**, 2760–2767.
21 J. Xu, S. H. Lai, M. Hu, S. M. Ge, R. C. Xie, F. Li, D. D. Hua, H. Xu, H. Zhou, R. Wu, J. T. Fu, Y. Qiu, J. He, C. Li, H. X. Liu, Y. F. Liu, J. Q. Sun, X. J. Liu and J. Luo, *Small Methods*, 2020, **4**, 2000567.
22 A. Zhang, Y. X. Liang, H. P. Li, S. L. Wang, Q. X. Chang, K. Y. Peng, Z. G. Geng and J. Zeng, *Nano Lett.*, 2021, **21**, 7789–7795.
23 Y. S. Yao, W. J. Yin, Z. K. Tang, Y. M. Xu, J. Y. Guo, J. X. Cao, H. Q. Wang and X. L. Wei, *J. Phys. Chem. C*, 2022, **126**, 1271–1280.
24 B. He, L. Jia, Y. Cui, W. Zhou, J. Sun, J. Xu, Q. Wang and L. Zhao, *ACS Appl. Energy Mater.*, 2019, **2**, 7655–7662.
25 H. Yang, H. Liu, X. Liu, Z. Zhao and J. Luo, *Catal. Sci. Technol.*, 2018, **8**, 5428–5433.
26 X. F. Yang, A. Wang, B. Qiao, J. Li, J. Liu and T. Zhang, *Acc. Chem. Res.*, 2013, **46**, 1740–1748.
27 C. Gao, S. M. Chen, Y. Wang, J. W. Wang, X. S. Zheng, J. F. Zhu, L. Song, W. K. Zhang and Y. J. Xiong, *Adv. Mater.*, 2018, **30**, 1704624.
28 S. Gao, Y. Lin, X. C. Jiao, Y. F. Sun, Q. Q. Luo, W. H. Zhang, D. Q. Li, J. L. Yang and Y. Xie, *Nature*, 2016, **529**, 68–71.
29 T. T. Zheng, K. Jiang, N. Ta, Y. F. Hu, J. Zeng, J. Y. Liu and H. T. Wang, *Joule*, 2019, **3**, 265–278.
30 C. Guo, T. Zhang, X. Deng, X. Liang, W. Guo, X. Lu and C. M. L. Wu, *ChemSusChem*, 2019, **12**, 5126–5132.
31 S. Back, J. Lim, N.-Y. Kim, Y.-H. Kimb and Y. Jung, *Chem. Sci.*, 2017, **8**, 1090–1096.
32 Z. X. Wang, J. X. Zhao and Q. H. Cai, *Phys. Chem. Chem. Phys.*, 2017, **19**, 23113–23121.
33 P. Hohenberg and W. Kohn, *Phys. Rev. B: Condens. Matter Mater. Phys.*, 1964, **136**, B864–B871.
34 W. Kohn and L. Sham, *Phys. Rev.*, 1965, **140**, A1133–A1138.
35 G. Kresse and D. Joubert, *Phys. Rev. B: Condens. Matter Mater. Phys.*, 1999, **59**, 1758.
36 G. Kresse and J. Furthmüller, *Phys. Rev. B: Condens. Matter Mater. Phys.*, 1996, **54**, 11169.
37 J. P. Perdew, K. Burke and M. Ernzerhof, *Phys. Rev. Lett.*, 1996, **77**, 3865–3868.
38 J. Perdew and Y. Wang, *Phys. Rev. B: Condens. Matter Mater. Phys.*, 1992, **45**, 13244–13249.
39 B. Hammer, K. W. Jacobsen and J. K. Nørskov, *Phys. Rev. Lett.*, 1993, **70**, 3971–3974.
40 S. Grimme, *J. Comput. Chem.*, 2006, **27**, 1787–1799.
41 H. J. Monkhorst and J. D. Pack, *Phys. Rev. B: Condens. Matter Mater. Phys.*, 1976, **13**, 5188–5192.
42 J. K. Nørskov, T. Bligaard, A. Logadottir, J. R. Kitchin, J. G. Chen, S. Pandelov and U. Stimming, *J. Electrochem. Soc.*, 2005, **152**, J23.
43 J. K. Nørskov, J. Rossmeisl, A. Logadottir, L. Lindqvist, J. R. Kitchin, T. Bligaard and H. Jonsson, *J. Phys. Chem. B*, 2004, **108**, 17886–17892.
44 V. Wang, N. Xu, J. C. Liu, G. Tang and W. T. Geng, *Comput. Phys. Commun.*, 2021, **267**, 108033.
45 J. Qiao, Y. Liu, F. Hong and J. Zhang, *Chem. Soc. Rev.*, 2014, **43**, 631–675.
46 S. Popovic, M. Smiljanic, P. Jovanovic, J. Vavra, R. Buonsanti and N. Hodnik, *Angew. Chem., Int. Ed.*, 2020, **59**, 14736–14746.
47 F. F. Xia and F. L. Yang, *Energy Fuels*, 2022, **36**, 4992–4998.
48 Z. Z. Chen, X. Zhang and G. Lu, *Chem. Sci.*, 2015, **6**, 6829–6835.
49 G. Luo, Y. Jing and Y. F. Li, *J. Mater. Chem. A*, 2020, **8**, 15809–15815.
50 M. G. Evans and M. Polanyi, *Trans. Faraday Soc.*, 1938, **34**, 11–24.
51 J. N. Bronsted, *Chem. Rev.*, 1928, **5**, 231–338.
52 X. Li, W. Bi, M. Chen, Y. Sun, H. Ju, W. Yan, J. Zhu, X. Wu, W. Chu and C. Wu, *J. Am. Chem. Soc.*, 2017, **139**, 14889–14892.
53 W. Bi, X. Li, R. You, M. Chen, R. Yuan, W. Huang, X. Wu, W. Chu, C. Wu and Y. Xie, *Adv. Mater.*, 2018, **30**, 1706617.
54 D. Kim, C. Xie, N. Becknell, Y. Yu, M. Karamad, K. Chan, E. J. Crumlin, J. K. Nørskov and P. Yang, *J. Am. Chem. Soc.*, 2017, **139**, 8329–8336.